Highly Conductive and Broadband Transparent Zr-Doped In₂O₃ as Front Electrode for Solar Cells

Monica Morales-Masis ⓘ, Esteban Rucavado, Raphäel Monnard, Loris Barraud, Jakub Holovský, Matthieu Despeisse, Mathieu Boccard, and Christophe Ballif

Abstract—Broadband transparent and highly conducting electrodes are key to avoid parasitic absorption and electrical losses in solar cells. Here, we propose zirconium-doped indium oxide (IO:Zr) as a transparent electrode intrinsically meeting both requirements and demonstrate its application as the front electrode in silicon heterojunction (SHJ) solar cells. The exceptional properties of this material rely on the combination of high-doping and high electron mobilities, achieving with this a wide optical band gap (3.5–4 eV), low free carrier absorption, and high lateral conductivity. A single film of IO:Zr has an electron mobility of 100 cm²/V·s with a carrier density of 2.5–3×10^{20} cm⁻³, resulting in a sheet resistance of around 25 Ω/sq for 100-nm-thick films. Their implementation as a front electrode in SHJ solar cells results in an important gain in current density as compared to the standardly used Sn-doped indium oxide. This is due to reduced parasitic absorption in both, the UV and IR, as confirmed by external quantum efficiency measurements. SHJ devices with the optimized IO:Zr front electrode, resulting in current densities of 40 mA/cm², a fill factor of 80%, and a conversion efficiency of 23.4%.

Index Terms—Electron mobility, heterojunctions, solar cells, silicon, transparent electrodes, wide band gap semiconductors, zirconium-doped indium oxide (IO:Zr).

I. Introduction

THE fabrication of ultratransparent and highly conductive transparent electrodes is one of the key milestones to reduce parasitic absorption losses in solar cells [1]–[4]. Hydrogenated indium oxides (IO:H, ICO:H, IWO:H)—with mobility values above 100 cm²/V·s and band gaps between 3.5 and 3.8 eV—lead the race of materials that present an excellent combination of broadband transparency and high conductivity [4], [5]. Such layers were advantageously employed in various solar cell technologies including silicon heterojunction (SHJ) [6]–[11]. One of the drawbacks of the hydrogenated indium-based transparent conducting oxides (TCOs) for the latter case is a degraded contact resistance with the Ag metal grids upon annealing [9]. The introduction of water during deposition also represents a drawback for upscaling the fabrication process to production. Amorphous InZnO (IZO) has been proposed as a high mobility TCO alternative, presenting the advantages of high-mobility values (60 cm²/V·s) with no need of annealing steps as well as the avoidance of water introduction during deposition. The drawback of IZO is its narrow band gap due to its intrinsic amorphous structure [12]. Due to its good properties in the as-deposited state, IZO has nevertheless become one of the reference TCOs in perovskites/silicon tandem cells [13], [14].

Here, we report the development of an ultratransparent and highly conductive zirconium (Zr)-doped indium oxide (In₂O₃:Zr, here called IO:Zr for simplification). The high conductivity of the films ($\sigma = 4200$ S/cm) is achieved by high doping and high mobility. The former originates from a combination of Zr⁴⁺ dopants and oxygen deficiencies [15]. The origin of high mobility has been proposed to be related to the high crystalline quality of the grains after annealing, and to a similar Zr⁴⁺ ionic size to that of In³⁺ [1]. The high transparency comes from the combination of a wide optical band gap—due to high free carrier densities (Burstein–Moss shift) and a low free-carrier absorption in the IR—due to the high mobility. In fact, it has also been proposed that the improved IR transmittance originates from a modification of the permittivity of the material by adding ZrO₂ [16].

We optimized IO:Zr for application as the front electrode in SHJ solar cells, and compare the solar cell properties to reference In-based electrodes, mainly Sn-doped indium oxide (ITO) and IO:H. As the fabrication of this high-performing electrode does not require the intentional introduction of water during deposition to achieve high mobilities, and its high conductivity will allow a reduction of this layer thickness by almost half, IO:Zr is a strong candidate for next-generation TCO in industrial production with reduced cost as compared to standard ITO [17], [18].

M. Morales-Masis is with the MESA+ Institute for Nanotechnology, University of Twente, Enschede 7500 AE, The Netherlands (e-mail: m.moralesmasis @utwente.nl).

E. Rucavado, R. Monnard, and M. Boccard are with the Institute of Microengineering, Photovoltaics and Thin-Film Electronics Laboratory, Ecole Polytechnique Fédérale de Lausanne, Neuchatel CH-2002, Switzerland (e-mail: esteban.rucavado@epfl.ch; raphael.monnard@epfl.ch; mathieu.boccard@epfl.ch).

L. Barraud and M. Despeisse are with the PV-Center, Swiss Center for Electronics and Microtechnology, Neuchatel CH-2002, Switzerland (e-mail: loris.barraud@csem.ch; Matthieu.DESPEISSE@csem.ch).

J. Holovský is with the Institute of Physics of the Czech Academy of Sciences, Prague 162 00, Czech Republic, and also with the Faculty of Electrical Engineering, Czech Technical University in Prague, Prague 166 27, Czech Republic (e-mail: holovsky@fzu.cz).

C. Ballif is with the Institute of Microengineering, Photovoltaics and Thin-Film Electronics Laboratory, Ecole Polytechnique Fédérale de Lausanne, Neuchatel CH-2002, Switzerland, and also with the PV-Center, Swiss Center for Electronics and Microtechnology, Neuchatel CH-2002, Switzerland (e-mail: christophe.ballif@epfl.ch).

Color versions of one or more of the figures in this paper are available online at http://ieeexplore.ieee.org.

Digital Object Identifier 10.1109/JPHOTOV.2018.2851306

This article has been accepted for inclusion in a future issue of this journal. Content is final as presented, with the exception of pagination.

2

IEEE JOURNAL OF PHOTOVOLTAICS

II. Experimental Details

The IO:Zr films were fabricated by RF sputtering from an In_2O_3:Zr target (98 wt% In_2O_3 and 2 wt% ZrO_2) at room temperature. The RF power density was 0.95 W/cm^2 and the oxygen to total flow ratio $r(O_2) = O_2/(Ar + O_2)$ introduced during the deposition was varied from 0.05% to 0.2%. All films were 100 ± 5 nm thick.

For the electrical and optical characterization of the films, the TCOs were deposited onto glass substrates, and for the photothermal deflection spectroscopy (PDS) measurements onto fused silica substrates. The TCOs were characterized before and after annealing (in air at 210 °C for 20 min), simulating the TCO properties after full SHJ solar cell fabrication [6].

The electrical resistivity (ρ), carrier concentration (N_e), and Hall mobility (μ_{Hall}) were measured by the Hall effect in the van der Pauw configuration. The optical transmittance (T) and reflectance (R) of the films were measured by a UV–vis–NIR spectrometer with an integrating sphere, and the absorptance was determined from 100-T-R.

PDS was performed by an in-house developed system based on a 150 W Xenon lamp. Fluorinert FC-72 was used as a temperature sensitive liquid. The absorption coefficient and refractive index were evaluated as described in [12].

SHJ cells were fabricated on a 240-μm-thick, 4-in, 3-Ω·cm, float-zone wafer, which was textured in a KOH-based solution, cleaned and dipped in 5% HF for one minute prior to loading for layer depositions. Plasma-enhanced chemical vapor deposition (PECVD) was used to deposit the intrinsic (i) and doped (p and n) amorphous silicon (a-Si:H) layers on each side. The p-type layer was deposited on the front (light-incoming) side of the wafer. The front TCO was then sputtered, and on the rear side, ITO and Ag were subsequently sputtered. Screen printing was used for the front Ag grid, and the device was finally cured at 210 °C for 20 min.

III. Results and Discussion: Optoelectronic Properties

A. Influence of the Oxygen Partial Pressure on the Optoelectronic Properties of IO:Zr Films

Optimization of the optoelectronic properties of the IO:Zr electrodes was performed by sputtering films from an In_2O_3/ZrO_2(98/2 wt%) target varying the oxygen content during deposition. The oxygen to total partial pressure during deposition is represented by $r(O_2) = O_2/(Ar + O_2)$. The target composition was chosen following [19]. All depositions were performed at room temperature and the base pressure in the system was $< 1e-6$ mbar just before deposition. It is important to emphasize here that no water is intentionally introduced in the system during deposition, contrary to the case of other high mobility TCOs, such as IO:H, IWO:H, and ICO:H [5], [11].

Fig. 1(a) shows the free carrier density (N_e) and Hall mobility (μ_{Hall}) as a function of $r(O_2)$ for the as-deposited films and after annealing at 200 °C in air for 20 min (this simulates the curing step of the Ag paste when applied in SHJ cells). A maximum N_e of 4×10^{20} cm^{-3} is found for $r(O_2) = 0.05\%$, whereas a maximum μ_{Hall} of 100 cm^2/V·s is found for $r(O_2) =$
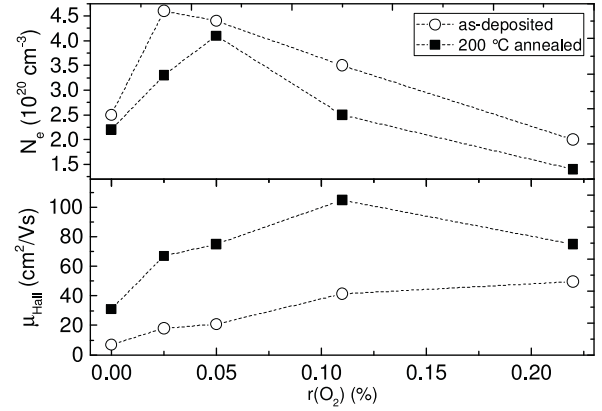

Fig. 1. Free carrier density (N_e) and Hall mobility (μ_{Hall}) for IO:Zr films grown with distinct oxygen partial pressures, $r(O_2)$.
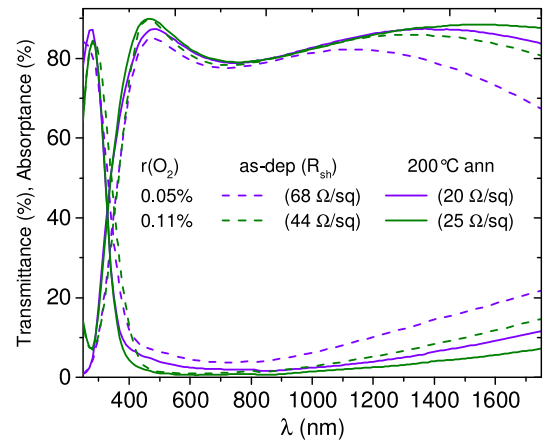

Fig. 2. UV–vis–NIR transmittance and absorptance spectra of 100-nm-thick IO:Zr films with the best electrical properties after annealing (see Fig. 1).

0.11%. All films are 100-nm-thick (measured on a flat substrate), corresponding to sheet resistances (R_{sheet}) of 20–25 Ω/sq for $r(O_2) = 0.05\%$ and 0.11%.

We can observe that, in general, oxygen tends to act against doping, saturating the oxygen vacancies. But this effect starts above $r(O_2) = 0.05\%$. An unknown competing effect is observed below this $r(O_2)$. Consequent increase of mobility with increasing $r(O_2)$ might be a typical consequence of concentration-dependent mobility as known for several oxide and nonoxide semiconductors [20]–[22].

Transmittance and absorptance spectra of the annealed films as a function of wavelength for different $r(O_2)$ are presented in Fig. 2. As expected, in the NIR–IR region, a clear reduction of free-carrier absorption is observed with decreasing N_e (increasing $r(O_2)$), while a blue shift is observed with decreasing $r(O_2)$. This blue shift and the corresponding band gap will be elaborated below.

B. Optical Band Gap

PDS with high sensitivity in the UV region was employed to measure the absorption coefficient (α) of the films and extract the optical band gaps. Assuming direct optical transitions, i.e., $n = 2$ in the Tauc relation $\alpha \propto (h\upsilon - E_g)^{1/n}$, an optical band
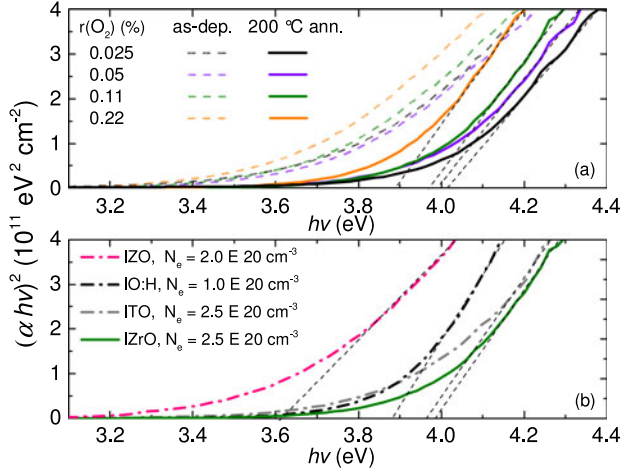
Fig. 3. (a) Tauc plot of IO:Zr films deposited with varying $r(O_2)$ for the as-deposited (colored dash lines) and annealed (solid lines) samples. (b) Comparison of the optical band gap of IO:Zr versus ITO, IO:H, and IZO. IO:Zr shows the widest band gap already for the film grown with 0.11% $r(O_2)$. Thin black dash lines in both graphs show the extrapolation used to extract the optical band gaps.

gap ranging from 3.9 up to 4 eV is obtained for the annealed samples [see Fig. 3(a)]. These correspond to values reported in the literature for polycrystalline IO:Zr films [23]. As observed in Fig. 3(a), for both, as-deposited and annealed samples, a slight blue shift with decreasing $r(O_2)$ is measured, which could be mainly attributed to the Burnstein–Moss shift [24]. A clear shift to wider band gaps is observed for the samples after annealing. This shift has been commonly attributed to crystallization of the In$_2$O$_3$-based films at temperatures above 150 °C [5], [25]. The transition from an amorphous to a crystalline phase after annealing the IO:Zr films at 200 °C has been recently confirmed by Rucavado *et al.* [26].

Fig. 3(b) presents a comparison of the IO:Zr film—0.11% $r(O_2)$—with IZO, IO:H, and ITO, which are widely used TCOs in SHJ cells [12]. Remarkably, IO:Zr films with $N_e > 2.5 \times 10^{20}$ cm^{-3} have the widest optical band gap from the series. Furthermore, these films also have very low free-carrier absorption in the IR (see Fig. 2), making these electrodes one of the best in terms of broad-band transparency. The broad-band transparency is moreover achieved by high N_e and μ, achieving high lateral conductivity and making them ideal to apply as the front electrode in solar cell devices with a broad-band absorption range, as SHJ cells.

C. Refractive Index

The refractive index (n) and extinction coefficient (k) of the annealed IO:Zr films with distinct N_e (see Fig. 1) are presented in Fig. 4. Changes in k and n are consistent with the role of oxygen acting against doping. Consequently, free-carrier absorption drops and bandgap narrows due to Burstein–Moss shift. Following the antireflecting coating conditions to maximized light in-coupling in textured silicon cells, an 80-nm-thick (on textured wafer) IO:Zr film should be sufficient to comply with this requirement [27]. It is nevertheless important to mention that based on the electrical properties and the geometry of a
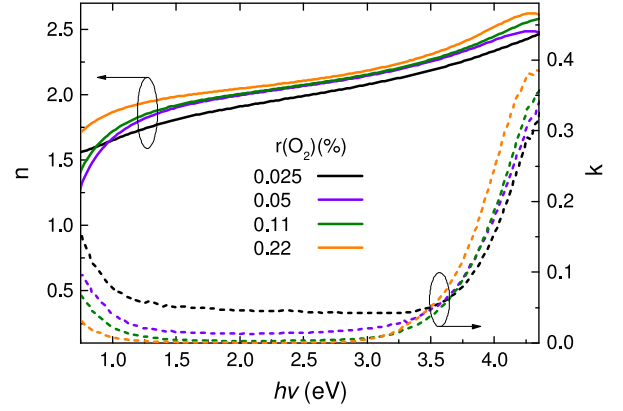

Fig. 4. Refractive index (n) and extinction coefficient (k) as a function of photon energy ($h\nu$) of IO:Zr thin films (annealed at 200 °C) with varying oxygen flow ratio $r(O_2)$.
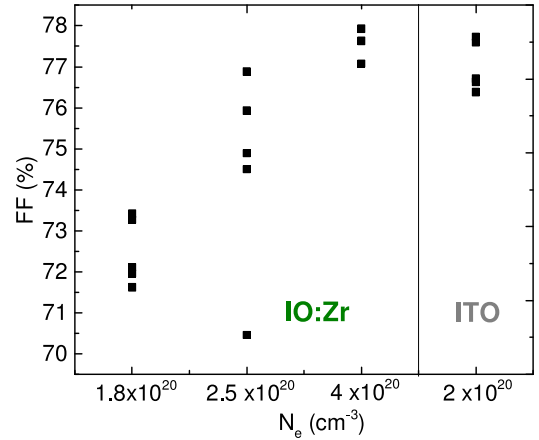

Fig. 5. Fill factor (FF) variation with increasing carrier density (N_e) of the IO:Zr front electrodes in SHJ solar cells. Comparison with the case of a standard ITO front electrode.

standard grid in SHJ cells, the layer of IO:Zr could be thinner, roughly half the thickness, while still reaching 100 Ω/sq of sheet resistance. A highly transparent layer with low refractive index could be applied to compensate the thickness necessary to match the ARC condition [28], [29]. Note also that in a module configuration, the ARC conditions are relaxed due to the larger refractive index of the encapsulant compared to air, making thinner layers optically advantageous [30].

IV. RESULTS AND DISCUSSION: APPLICATION IN SHJ SOLAR CELLS

A. Fill Factor Dependence With IO:Zr Free Carrier Density

Fig. 5 presents the fill factor (FF) variation when applying IO:Zr with distinct N_e as the front electrode in SHJ solar cells. For this initial experiment, 40-nm-thick IO:Zr layers were used (instead of the standard 80-nm-thick for optimized ARC), and compared with 80-nm-thick baseline ITO (electrical properties in Table I). Notice that due to the high mobility of IO:Zr, R_{sheet} of the 40-nm-thick films compares better to 100 Ω/sq of the ITO. A clear FF improvement is observed with increasing N_e

TABLE I
ELECTRICAL PROPERTIES OF IO:ZR, IO:H, AND ITO FRONT ELECTRODES AND SHJ SOLAR CELL RESULTS FOR EACH OF THE FRONT ELECTRODES

Optimized Properties	In_2O_3:Zr (IO:Zr)	In_2O_3:H (IO:H)	In_2O_3:Sn (ITO)
N (cm^{-3})	2.5×10^{20}	1×10^{20}	2×10^{20}
μ (cm^2/Vs)	100	110	30
R$_{sheet}$ for 100 nm (Ω/□)	25	50	100
Contact resistance with Ag (Ohm.cm^2)	$< 1.10^{-4}$	$> 1.10^{-4}$ (depends on water content) [9]	$< 1.10^{-4}$
N (cm^{-3})	2.5×10^{20}	1×10^{20}	2×10^{20}
V$_{oc}$ (mV)	725 (727)[*]	726 (727)	724 (727)
FF (%)	79.4 (80.5)[*]	80.6 (81.0)	80.3 (81.5)
J$_{sc}$ (mA/cm^2)	40.0 (40.2)[*]	39.7 (39.9)	39.5 (39.7)
Efficiency (%)	23.0 (23.4)[*]	23.2 (23.4)	23.0 (23.4)

[*]The values in parenthesis are the best cell. The values outside the parenthesis are the average of five cells. Cell area is 2×2 cm^2.
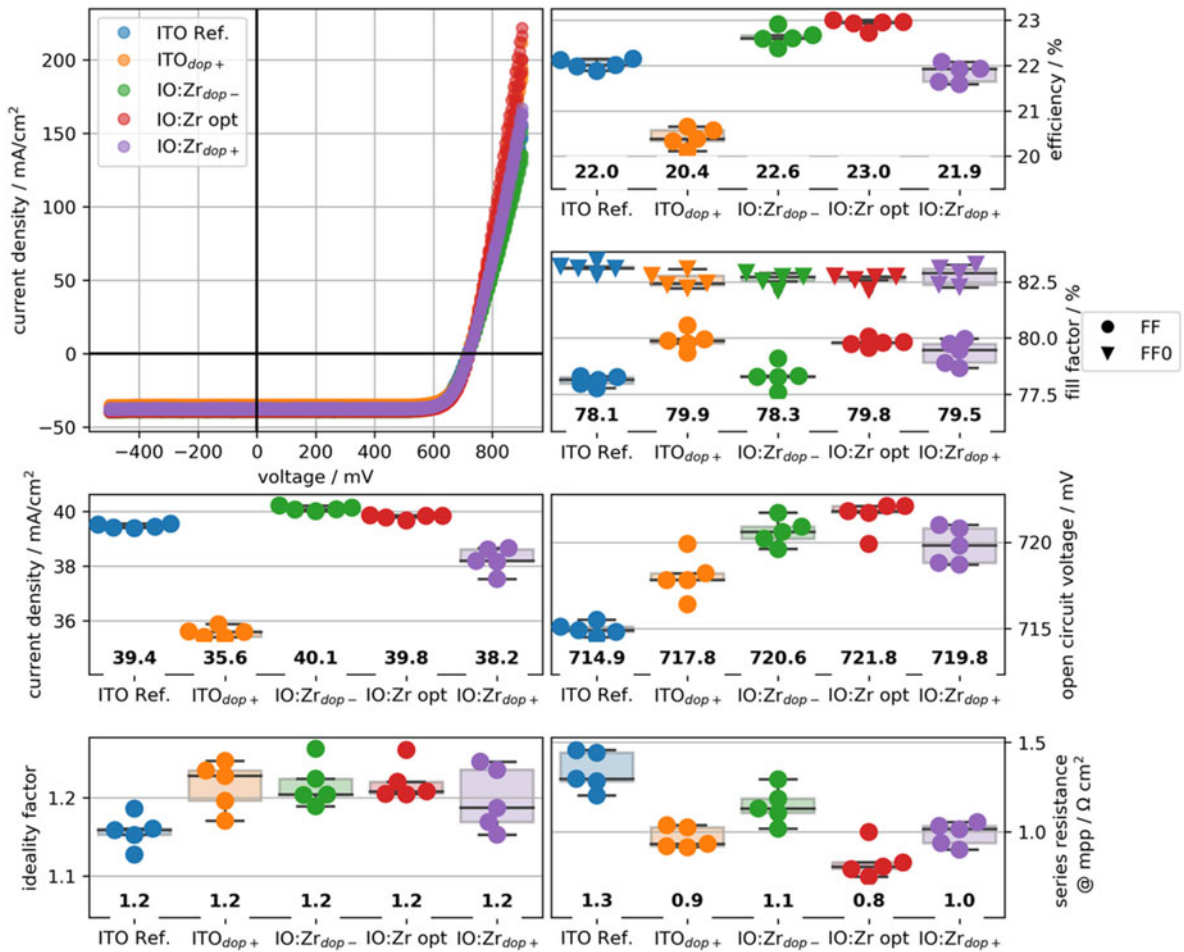

Fig. 6.   *IV* performance of standard heterojunction solar cells implementing either a standard ITO layer (ITO ref) as a front TCO, a highly doped ITO (ITO$_{dop+}$), or an IO:Zr film with homogeneous low doping (IO:Zr$_{dop-}$), bilayer high/low doping (IO:Zr opt), or homogeneous high doping (IO:Zr$_{dop+}$). IO:Zr opt layer with an N_e gradient aims at reduced contact resistance (higher interface doping) and the higher oxygen content for the bulk of the layer leads to reduce parasitic absorption. Additionally to usual parameters, FF$_0$ and the maximum-power-point series resistance were extracted from variable-illumination *IV* curves and show that the low-doping (IO:Zr$_{dop--}$) and IO:Zr with N_e gradient (IO:Zr opt) exhibit lower series resistance than the reference ITO. To reach similar series resistance with ITO, a strongly doped (thus absorbing) layer has to be used (ITO$_{dop+}$), which drastically lowers J_{sc}.
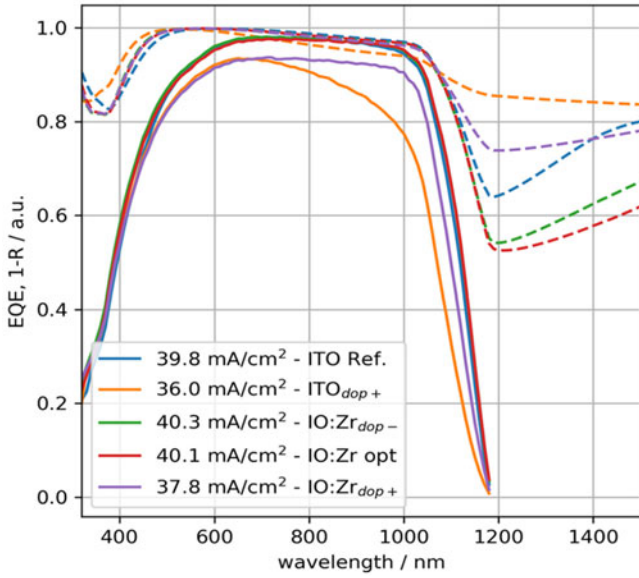
This article has been accepted for inclusion in a future issue of this journal. Content is final as presented, with the exception of pagination.

MORALES-MASIS *et al.*: HIGHLY CONDUCTIVE AND BROADBAND TRANSPARENT ZR-DOPED IN$_2$O$_3$ AS FRONT ELECTRODE

5

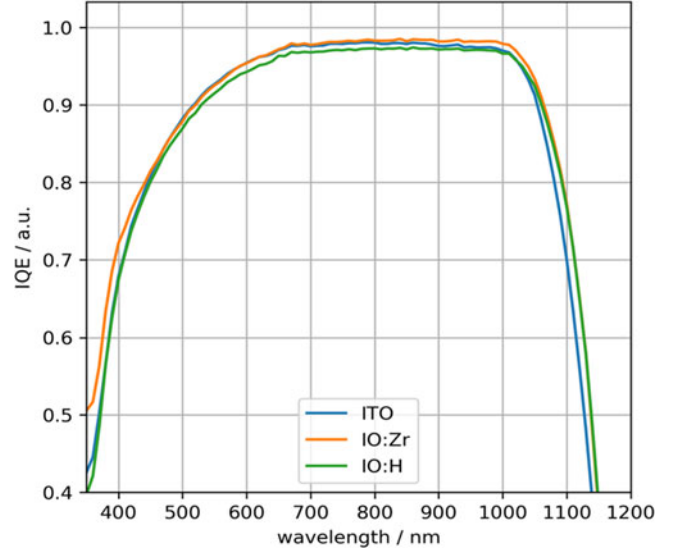Fig. 7.   EQE and total absorption $(1 - R)$ of the solar cells discussed in Fig. 6.

Fig. 8.   Internal quantum efficiency (IQE) of front emitter SHJ solar cells with high mobility IO:Zr and comparison with IO:H and ITO cells. The advantage of IO:Zr is evident by the improved spectral response in the UV–vis in comparison to IO:H and ITO, and the high IR transmittance matching that of IO:H.

in IO:Zr, overpassing that of ITO at N_e above 4×10^{20} cm^{-3}. As the film with such high N_e has a higher absorptance than the highest mobility film ($N_e = 2.5 \times 10^{20}$ cm^{-3}), we introduce in the following part a bilayer approach: starting with a buffer layer of high N_e at the interface with the a-Si:H(p) and completing the film with the high mobility film.

B. IO:Zr With Free Carrier Density Gradient as the Front Electrode in SHJ Solar Cells

Fig. 6 shows solar cell results for devices using ITO and IO:Zr. Three different IO:Zr are compared: *IO:Zr opt* (films with a N_e gradient from 4.5×10^{20} cm^{-3} at the interface with a-Si:H(p) down to 2.5×10^{20} cm^{-3} and 100 cm^2/V·s at the bulk of the film, *IO:Zr*$_{\text{dop}-}$ (a single layer with homogeneous doping of 2.5×10^{20} cm^{-3}), and *IO:Zr*$_{\text{dop}+}$ (a single layer with homogeneous doping of 4.5×10^{20} cm^{-3}). Two types of ITOs are also compared: a reference ITO used in baseline SHJ cells (*ITO ref*) (properties in Table I) and a highly doped ITO (*ITO*$_{\text{dop}+}$). All films are 80-nm-thick on the textured wafer.

For cells with *IO:Zr opt*, all performance parameters are improved compared to the reference ITO. Better open-circuit voltages (V_{oc}) can possibly be linked to reduced sputter-induced damage, higher J_{sc} to lower parasitic absorption (both in the short and long wavelength ranges, see Fig. 7), and higher FF to lower series resistance from lower sheet resistance $\sim$50 Ω/sq compared to $\sim$120 Ω/sq for the *ITO ref*. The *ITO*$_{\text{dop}+}$ shows similar sheet resistance ($\sim$50 Ω/sq) but clearly exhibits higher parasitic absorption (see J_{sc} and Figs. 6 and 7). The overall efficiency obtained with the best single-layer TCO *IO:Zr*$_{\text{dop}-}$ is 0.6% higher than for the *ITO ref*, and with the optimal process (with N_e gradient) *IO:Zr opt* it is even 1% absolute higher reaching 23.0%. This is achieved without any second antireflective (AR) layer, using standard PECVD layers and screen printing (area is 2×2 cm^2 with external busbars).

C. IO:Zr as the Front Electrode in High-Efficiency SHJ Solar Cells

The IO:Zr front electrodes have been furthermore applied in similar SHJ devices, optimized for higher efficiencies as compared to the cells presented in Figs. 6 and 7, relying on finer tuning of the a-Si:H layers. Interestingly for this type of cells, the best results were obtained for the single IO:Zr film with homogeneous doping and high mobility (IO:Zr$_{\text{dop}-}$). This resulted in the best J_{sc} of 40.2 mA/cm^2 compared to IO:H and ITO. Fig. 8 shows the improved spectral response in the UV–vis of the IO:Zr cells in comparison to IO:H and ITO, and the high IR transmittance matching that of IO:H. An FF drop of $\sim$1% is observed, which was not improved by applying the N_e gradient as shown above. Further investigations are required to determine the cause of this drop, which we attribute to the (p)a-Si:H/IO:Zr interface. This highlights the fact that even slight differences in terms of doped layers require adapting the TCO layer when targeting very high efficiencies. Finally, we demonstrate that an efficiency of 23.4% can be achieved with IO:Zr, the same as the case of IO:H and ITO.

Note that the grid design does not account for the higher sheet conductance of the IO:Zr layer and was optimized for the ITO case. There is, thus, a clear potential of IO:Zr to further enhance J_{sc} by optimizing the front metal grid or reducing the thickness in half (doubling R_{sheet}) to further push the limits of transparency of the material. Reducing the thickness is as well important to reduce the amount of indium used in cells, reducing the cost and depletion of nonabundant elements in the Earth crust.

V. CONCLUSION

The broadband transparency of IO:Zr makes this material an excellent candidate to replace ITO and enhance the efficiency of cells with a wide spectral response. We demonstrated a clear

gain in current density with respect to reference cells with ITO, by simply applying the IO:Zr and keeping the same metal front grid. Further gain can be reached by reducing the thickness of the IO:Zr layer, pushing the limits of transparency of the material or increasing the separation of the front metal fingers, as R_{sheet} of IO:Zr is much lower than the ITO for which the grid has been optimized.

Additional advantages of IO:Zr are its simple processing, namely, the fact that water is not intentionally introduced during deposition and the room temperature deposition with only an annealing step at a modest temperature of 200 °C.

We propose the use of the IO:Zr front electrode with a free carrier density gradient (high to low doping) to improve the FF in SHJ cells with lowly conductive a-Si:H (p) layers. However, when using different a-Si:H (i) and (p) layers in the cells, a single high mobility IO:Zr with homogeneous doping is sufficient to achieve conversion efficiencies of 23.4%, as demonstrated in this work. IO:Zr is furthermore potentially interesting for applications as perovskite/SHJ or perovskite/CIGS tandem solar cells, where the transparency of the front electrode is of crucial importance. Due to its low-temperature processing, IO:Zr also has potential applications in flexible optoelectronic devices, such as flexible OLEDs or solar cells deposited on temperature-sensitive polymer substrates.

REFERENCES

[1] S. Calnan and A. N. Tiwari, "High mobility transparent conducting oxides for thin film solar cells," *Thin Solid Films*, vol. 518, no. 7, pp. 1839–1849, 2010.

[2] Z. C. Holman *et al.*, "Infrared light management in high-efficiency silicon heterojunction and rear-passivated solar cells," *J. Appl. Phys.*, vol. 113, no. 1, 2013, Art. no. 013107.

[3] M. Boccard, N. Rodkey, and Z. C. Holman, "High-mobility hydrogenated indium oxide without introducing water during sputtering," *Energy Procedia*, vol. 92, pp. 297–303, Aug. 2016.

[4] M. Morales-Masis, S. De Wolf, R. Woods-Robinson, J. W. Ager, and C. Ballif, "Transparent electrodes for efficient optoelectronics," *Adv. Electron. Mater.*, vol. 3, no. 5, 2017, Art. no. 1600529.

[5] T. Koida, Y. Ueno, and H. Shibata, "In-based transparent conducting oxide films with high electron mobility fabricated at low process temperatures," *Phys. Status Solidi, Appl. Mater. Sci.*, vol. 215, 2018, Art. no. 1700506.

[6] T. Koida, H. Fujiwara, and M. Kondo, "Reduction of optical loss in hydrogenated amorphous silicon/crystalline silicon heterojunction solar cells by high-mobility hydrogen-doped in 2O3 transparent conductive oxide," *Appl. Phys. Express*, vol. 1, no. 4, 2008, Art. no. 041501.

[7] T. Koida, H. Sai, and M. Kondo, "Application of hydrogen-doped In2O3 transparent conductive oxide to thin-film microcrystalline Si solar cells," *Thin Solid Films*, vol. 518, no. 11, pp. 2930–2933, 2010.

[8] C. Battaglia *et al.*, "Micromorph thin-film silicon solar cells with transparent high-mobility hydrogenated indium oxide front electrodes," *J. Appl. Phys.*, vol. 109, no. 11, 2011, Art. no. 114501.

[9] L. Barraud *et al.*, "Hydrogen-doped indium oxide/indium tin oxide bilayers for high-efficiency silicon heterojunction solar cells," *Sol. Energy Mater. Sol. Cells*, vol. 115, pp. 151–156, 2013.

[10] Y. E. Romanyuk *et al.*, "Hydrogenated indium oxide window layers for high-efficiency Cu(In,Ga)Se 2 solar cells," *J. Appl. Phys.*, vol. 117, 2015, Art. no. 205301.

[11] E. Kobayashi, Y. Watabe, T. Yamamoto, and Y. Yamada, "Cerium oxide and hydrogen co-doped indium oxide films for high-efficiency silicon heterojunction solar cells," *Sol. Energy Mater. Sol. Cells*, vol. 149, pp. 75–80, 2016.

[12] M. Morales-Masis, S. Martin De Nicolas, J. Holovsky, S. De Wolf, and C. Ballif, "Low-temperature high-mobility amorphous IZO for silicon heterojunction solar cells," *IEEE J. Photovolt.*, vol. 5, no. 5, pp. 1340–1347, Sep. 2015.

[13] J. Werner *et al.*, "Sputtered rear electrode with broadband transparency for perovskite solar cells," *Sol. Energy Mater. Sol. Cells*, vol. 141, pp. 407–413, 2015.

[14] J. Werner, B. Niesen, and C. Ballif, "Perovskite/silicon tandem solar cells: Marriage of convenience or true love story? – An overview," *Adv. Mater. Interfaces*, vol. 5, no. 1, 2018, Art. no. 1700731.

[15] T. Koida and M. Kondo, "High-mobility transparent conductive Zr-doped in2O3," *Appl. Phys. Lett.*, vol. 89, no. 8, pp. 87–90, 2006.

[16] T. A. Gessert, J. Burst, X. Li, M. Scott, and T. J. Coutts, "Advantages of transparent conducting oxide thin films with controlled permittivity for thin film photovoltaic solar cells," *Thin Solid Films*, vol. 519, no. 21, pp. 7146–7148, 2011.

[17] A. Louwen, W. Van Sark, R. Schropp, and A. Faaij, "A cost roadmap for silicon heterojunction solar cells," *Sol. Energy Mater. Sol. Cells*, vol. 147, pp. 295–314, 2016.

[18] S. C. Dixon, D. O. Scanlon, C. J. Carmalt, and I. P. Parkin, "n-Type doped transparent conducting binary oxides: An overview," *J. Mater. Chem. C*, vol. 4, no. 29, pp. 6946–6961, 2016.

[19] T. Koida and M. Kondo, "Improved near-infrared transparency in sputtered in2O 3-based transparent conductive oxide thin films by Zr-doping," *J. Appl. Phys.*, vol. 101, no. 6, pp. 4–8, 2007.

[20] D. M. Caughey and R. E. Thomas, "Carrier mobilities in silicon empirically related to doping and field," *Proc. IEEE*, vol. 55, no. 12, pp. 2192–2193, Dec. 1967.

[21] E. Rucavado *et al.*, "Enhancing the optoelectronic properties of amorphous zinc tin oxide by subgap defect passivation: A theoretical and experimental demonstration," *Phys. Rev. B*, vol. 95, no. 24, 2017, Art. no. 245204.

[22] J. E. Medvedeva, D. B. Buchholz, and R. P. H. Chang, "Recent advances in understanding the structure and properties of amorphous oxide semiconductors," *Adv. Electron. Mater.*, vol. 3, 2017, Art. no. 1700082.

[23] H. Kim *et al.*, "Transparent conducting Zr-doped In2O3 thin films for organic light-emitting diodes," *Appl. Phys. Lett.*, vol. 78, no. 8, pp. 1050–1052, 2001.

[24] J. I. Pankove, *Optical Processes in Semiconductors*. New York, NY, USA: Dover, 1971.

[25] H. F. Wardenga, M. V. Frischbier, M. Morales-Masis, and A. Klein, "In situ hall effect monitoring of vacuum annealing of In2O3:H thin films," *Materials*, vol. 8, no. 2, pp. 561–574, 2015.

[26] E. Rucavado *et al.*, "Carrier transport mechanisms in Zr-doped indium oxide: Towards ultra-thin high-performing electrodes," submitted for publication.

[27] S. De Wolf, A. Descoeudres, Z. C. Holman, and C. Ballif, "High-efficiency silicon heterojunction solar cells: A review," *Green*, vol. 2, no. 1, pp. 7–24, 2012.

[28] E. Kobayashi *et al.*, "Amorphous gallium oxide grown by low-temperature PECVD," *J. Vac. Sci. Technol. A, Vac., Surf., Film*, vol. 36, no. 2, 2018, Art. no. 021518.

[29] S. Y. Herasimenka, W. J. Dauksher, M. Boccard, and S. Bowden, "ITO/SiOx:H stacks for silicon heterojunction solar cells," *Sol. Energy Mater. Sol. Cells*, vol. 158, pp. 98–101, 2016.

[30] S. C. McIntosh and K. R. Baker-Finch, "OPAL 2: Rapid optical simulation of silicon solar cells," in *Proc. 38th IEEE Photovolt. Spec. Conf.*, 2012, pp. 000265–000271.